PNAS RESEARCH ARTICLE | NEUROSCIENCE ENGINEERING OPEN ACCESS

Modulation of deep neural circuits with sonogenetics

Quanxiang Xian[a,1], Zhihai Qiu[a,b,1], Suresh Murugappan[a], Shashwati Kala[a], Kin Fung Wong[a], Danni Li[a], Guofeng Li[c], Yizhou Jiang[a], Yong Wu[a], Min Su[a], Xuandi Hou[a], Jiejun Zhu[a,b], Jinghui Guo[a], Weibao Qiu[c], and Lei Sun[a,2]

Edited by Lily Jan, HHMI–University of California San Francisco, San Francisco, CA; received December 3, 2022; accepted April 14, 2023

Noninvasive control of neuronal activity in the deep brain can be illuminating for probing brain function and treating dysfunctions. Here, we present a sonogenetic approach for controlling distinct mouse behavior with circuit specificity and subsecond temporal resolution. Targeted neurons in subcortical regions were made to express a mutant large conductance mechanosensitive ion channel (MscL-G22S), enabling ultrasound to trigger activity in MscL-expressing neurons in the dorsal striatum and increase locomotion in freely moving mice. Ultrasound stimulation of MscL-expressing neurons in the ventral tegmental area could activate the mesolimbic pathway to trigger dopamine release in the nucleus accumbens and modulate appetitive conditioning. Moreover, sonogenetic stimulation of the subthalamic nuclei of Parkinson's disease model mice improved their motor coordination and mobile time. Neuronal responses to ultrasound pulse trains were rapid, reversible, and repeatable. We also confirmed that the MscL-G22S mutant is more effective to sensitize neurons to ultrasound compared to the wild-type MscL. Altogether, we lay out a sonogenetic approach which can selectively manipulate targeted cells to activate defined neural pathways, affect specific behaviors, and relieve symptoms of neurodegenerative disease.

sonogenetics | ultrasound | MscL-G22S | neuromodulation | neural circuits

Significance

Manipulating specific neural activity by physical intervention is a powerful method to gain causal insight into brain functions and treat brain disorders. Sonogenetics is among the promising modalities being used to stimulate neurons noninvasively in the intact brain. Here, we demonstrate sonogenetics, a noninvasive neural stimulation approach using mechanosensitive ion channels, to control well-defined deep neural circuits and ameliorate parkinsonian motor behaviors through transcranial ultrasound stimulation. This sonogenetic approach may enhance our understanding of cell pathophysiology and lead to the development of unique treatments for neuropsychiatric diseases and nonneural diseases.

It has been a long-standing goal of neuroscience to specifically manipulate neural activity to understand the brain's functions and treat dysfunctions. In recent years, several forms of energy have been harnessed in order to stimulate neurons in the brain, the most prominent example being optogenetics. Another modality being studied for this purpose is ultrasound, such as ultrasound-alone approaches or combined with micro- or nanobubbles or heterologous ion channels. Sonogenetics, analogous to optogenetics, combines the targeted expression of mechanosensitive cellular machinery (e.g., ion channels) and precise delivery of ultrasound (US). This approach has been shown to enable noninvasive stimulation with high spatiotemporal resolution and accurate deep-brain targeting through cell type-specific gene expression (1–7) and could potentially be translated to application in large mammals, and possibly even humans.

"Sonogenetics" was first described in a study showing that, in the presence of microbubbles, ultrasound could activate specific neurons overexpressing the mechanosensitive ion channel TRP-4 to control the behaviors of *Caenorhabditis elegans* worms (2). Subsequent proof-of-concept studies have used different candidate molecules to enhance neuronal response to ultrasound stimulation, including the mechanosensitive proteins Prestin (3), MscL (1, 8), and hsTRPA1 (6). The MscL channel is a particularly intriguing candidate as it is a mechanically activated ion channel that can quickly convert mechanical stimuli into neuronal responses (9), independent of membrane potential (8), and other endogenous factors and thermal deposition (10). It has been reported that inducing MscL expression can enhance the ability of ultrasound to stimulate cells (8). Indeed, our previous work shows that the expression of MscL in mice can sensitize neurons to ultrasound and induce neuronal activation in a targeted region, expressing it without influencing the resting membrane potential of neurons (1).

Thus far, the MscL channel has proved to be a good choice as an effector molecule for sonogenetic-based neurostimulation at cellular level. However, for manipulating higher-order processes, such as specific behaviors or complex phenomena like decision-making or emotion, a spatiotemporally coordinated activation of specific neural networks is required (11). To progress over the proof-of-concept stage, direct evidence of sonogenetics' ability to coordinate the activation of specific neural circuits and behavioral outcomes is required, given the possibility of confounding elements such as endogenous mechanosensitive ion channels or a nonspecific auditory effect triggered by ultrasound. This requires the temporal resolution of sonogenetic stimulation in vivo to be recorded directly from the neurons being targeted. This information would allow the effects of the stimulation to be better understood and, in turn, allow greater fine-tuning of parameters and protocols for maximum efficacy. Given the significant advantage that ultrasound provides, in that it can be delivered

Author contributions: Q.X., Z.Q., J.G., and L.S. designed research; Q.X., Z.Q., S.M., S.K., K.F.W., D.L., G.L., Y.J., Y.W., M.S., X.H., J.Z., and W.Q. performed research; L.S. contributed new reagents/analytic tools; Q.X., Z.Q., S.M., K.F.W., D.L., X.H., and J.G. analyzed data; and Q.X., Z.Q., S.K., and L.S. wrote the paper.

The authors declare no competing interest.

This article is a PNAS Direct Submission.

[1]Q.X. and Z.Q. contributed equally to this work.

[2]To whom correspondence may be addressed. Email: lei.sun@polyu.edu.hk.

This article contains supporting information online at https://www.pnas.org/lookup/suppl/doi:10.1073/pnas.2220575120/-/DCSupplemental.

Published May 22, 2023.

transcranially and noninvasively, it holds promise for eventual clinical transition, which makes it important to understand and validate the ability of the sonogenetic approach to modulate specific circuits in the brain.

Here, we report an MscL-G22-mediated sonogenetic approach (MscL-sonogenetics) to activate specific neurons in intact mouse brains, modulating well-defined neural circuits and inducing corresponding behaviors in freely moving mice. We demonstrate the capability of sonogenetics to activate targeted neurons in different subcortical brain regions, including the dorsal striatum (dSTR) and ventral tegmental area (VTA). MscL-sonogenetic stimulation of these regions was found to selectively activate the targeted neural circuits quickly as measured by fiber photometry (FP) and could specifically induce asymmetric locomotion and appetitive conditioning behavior. Spatial specificity was verified by observing upregulation of the neural activation marker c-Fos, and neuronal responses showed subsecond latency. Finally, MscL-mediated stimulation of the subthalamic nucleus (STN) in a mouse Parkinson's disease (PD) model could relieve motor symptoms and improve the movement coordination of mice. Our functional and behavioral experiments showed that MscL expression significantly enhanced neuronal activation by low-frequency noninvasive ultrasound without the need for intracranial implants or microbubbles.

Results

MscL-Sonogenetic Stimulation of dSTR Neurons Induces Motor Response in Mice. In a previous study, we used the MscL channel to mediate ultrasound neurostimulation of targeted neurons in the mouse primary motor cortex and dorsomedial striatum (1). Short ultrasound pulse train of 300 ms at low intensities was sufficient to trigger neuronal activation, determined by c-Fos expression and forelimb muscle contractions. Here, we decided to build upon these data and evaluate whether our previously used protocol was effective and specific enough to also trigger immediate and direct neural activation and corresponding movement behaviors in awake mice. We chose the dSTR as our target because it is a relatively deep region (located ~2.75 mm below the skull) with a well-defined function and behavioral pattern, which is relative to initiate and control movement of the body (12–16). Specifically, it is expected to induce asymmetric locomotion when the neurons are activated.

We examined the direct effect of MscL-sonogenetics on dSTR neuronal activation by measuring fluorescence changes of jRGECO1a (genetically encoded calcium sensor with red fluorescence) (17) in real time using FP. Neurons in the right dSTR were simultaneously transduced by hSyn-promoted jRGECO1a and EYFP-only, wild-type-MscL (MscL-WT)-EYFP, or MscL-G22S-EYFP AAVs (Fig. 1*A*). We observed robust expression of EYFP and jRGECO1a colocalized in dSTR neurons (Fig. 1*B*). Four to five weeks posttransduction, the mice were transcranially stimulated with short US pulse train (parameters shown in Fig. 1*C* and acoustic intensity profile shown in *SI Appendix*, Fig. S1) and an optical fiber was used to monitor fluorescence intensity. Prior to US stimulation, both groups showed comparable levels of baseline fluorescence (peak $\Delta F/F_0$ for EYFP = 1.21 ± 0.31%, MscL-WT = 1.35 ± 0.24%, and MscL-G22S = 1.77 ± 0.47%, Fig. 1 *D* and *E*). However, upon delivery of one 0.05 MPa pressure US pulse train, MscL-G22S-expressing neurons showed a rapid and significant increase in jRGECO1a fluorescence intensity compared to EYFP-only or MscL-WT neurons (peak $\Delta F/F_0$ for EYFP = 1.85 ± 0.52%, MscL-WT = 1.37 ± 0.23%, MscL-G22S = 4.857 ± 1.47%, Fig. 1*D*). Fluorescence responses to US in the MscL-G22S dSTR regions were 2.63-fold of the response from the EYFP dSTR. Acoustic pressures from 0.05 MPa to 0.2 MPa reliably evoked dSTR neural activity in MscL-G22S mice, and a generalized pattern of dose dependence was observed (Fig. 1*E*). In contrast, the EYFP- or MscL-WT-expressing mice showed a small fluorescence change comparable to spontaneous activity after US stimulation. The latency range of neuronal responses in MscL-G22S-expressing neurons was 327.3 ±29.05 ms to 341.7 ± 21.65 ms (Fig. 1*F*).

To test whether local temperature induced by sonication may participate in the neuronal activation, we conducted a computer simulation to calculate the temperature increase with our sonication parameters. The focal temperature elevation in our protocol was less than 0.2 °C (*SI Appendix*, Fig. S2), suggesting that the thermal effect was not a main contributor.

To further evaluate the spatial targeting of our scheme, anesthetized mice were treated with US for 40 min and their brains were stained for the neural activation marker, c-Fos. Robust EYFP expression was seen in the dSTR of both EYFP-only and MscL-G22S mice (Fig. 1*G*). The average c-Fos expression in dSTR was found to be significantly higher in the stimulated side of the MscL-G22S mice (87 ± 8 c-Fos$^+$ cells) than that in the contralateral side of the same mice (11 ± 2 c-Fos$^+$ cells) or in mice expressing only EYFP (stimulation side = 14 ± 3, contralateral = 8 ± 2 c-Fos$^+$ cells) (Fig. 1*H*). Crucially, we found that the cortical regions located directly above the dSTR on the stimulation side did not show a significantly higher level of c-Fos (Fig. 1*H*). This indicated that our setup was able to focus the effects of US in the region expressing MscL-G22S and not surrounding areas, consistent with our previous results (1). This is especially important because a single-element plane transducer with a diameter of 5 mm was used, meaning that the cortical neurons above the dSTR were unavoidably sonicated as the ultrasonic waves propagated through the brain. The upregulation of c-Fos being restricted to the region of MscL-G22S expression clearly demonstrates the gain-of-function role of the mechanosensitive mediator in sonogenetics. We also stained for c-Fos in the auditory cortex of the brain slices and observed comparable c-Fos between EYFP and MscL-G22S mice (*SI Appendix*, Fig. S3). Thus, we confirmed that MscL-sonogenetics could specifically activate neurons in the targeted dSTR of anesthetized mice.

We next tested whether the MscL-sonogenetics was effective enough to modulate the expected asymmetric locomotion in freely moving mice. A wearable US transducer was attached above the virally transduced dSTR in freely moving mice and their locomotion was recorded during US stimulation (Fig. 2 *A* and *B*). To prevent indirect activation of the auditory pathway rather than direct activation of motor circuits in awake mice, we sonicated the animals with both rectangular waveform and smooth waveform envelope (Fig. 2*C*), given the smooth waveform of ultrasound stimulation has been shown to minimize the auditory confound (18). Robust EYFP or MscL-G22S-EYFP signals were observed in the right dSTR region (Fig. 2*D*), confirming successful viral expression. The mice were then treated with ultrasound in an open field box and their movement behaviors were recorded and analyzed. Ultrasound stimulation consisted of three epochs [prestimulation ("Pre"), ultrasound stimulation ("US"), poststimulation ("Post")]. MscL-G22S-expressing mice were seen to obviously increase their locomotion activity during both rectangular and smooth waveform ultrasound treatment, compared to negligible change for EYFP mice (Fig. 2*E*). The mobility speed of the MscL-G22S mice increased, while the EYFP mice did not show obvious change (Fig. 2 *F* and *H*). MscL-G22S mice moved greater distances during the periods of US stimulation than those of EYFP mice (Fig. 2 *G* and *I*). EYFP mice also showed small increases in their motor activity during higher US stimulation, but the magnitude of these changes was small. Stimulation with smooth

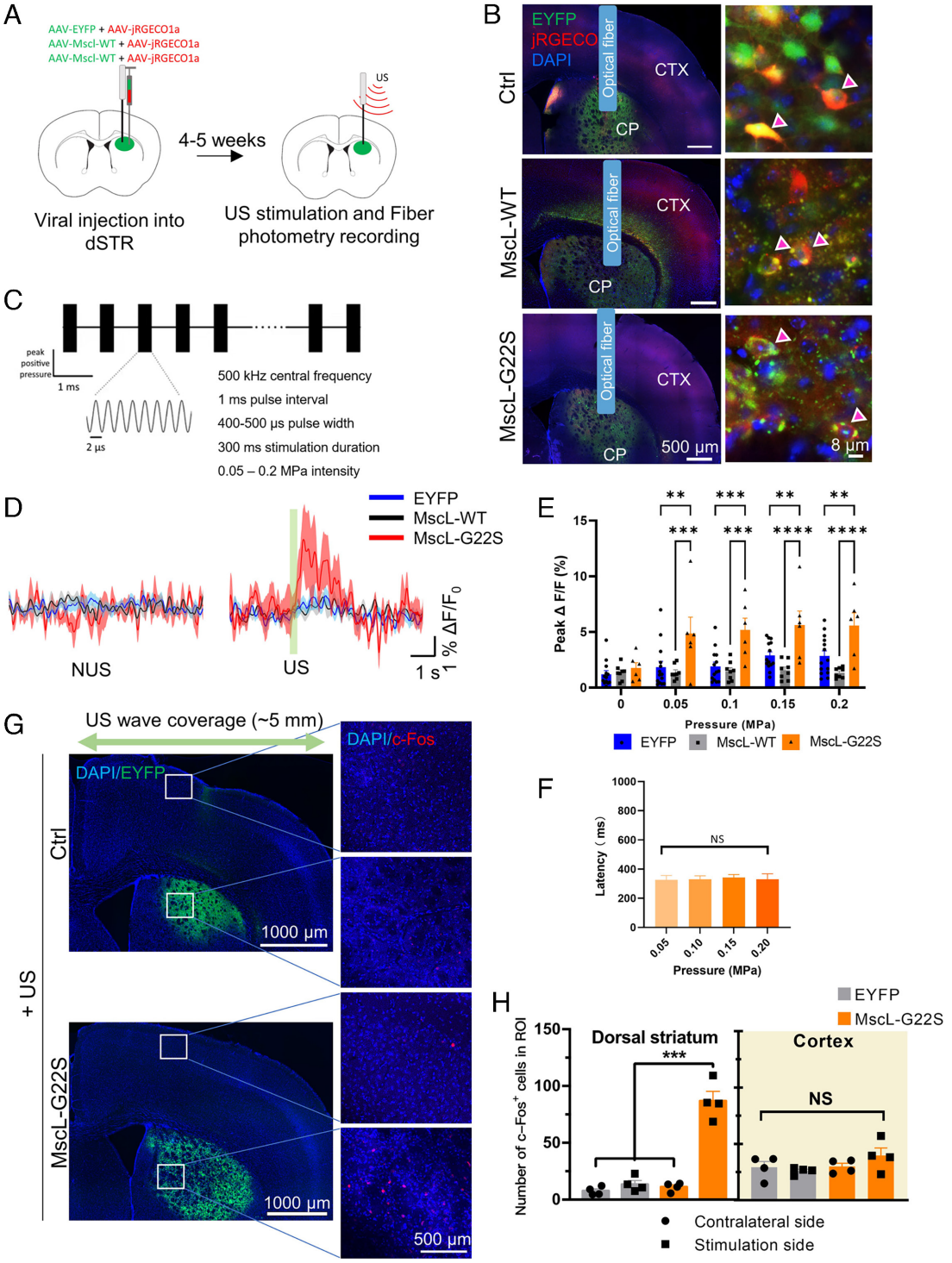

Fig. 1. MscL-sonogenetics enables specific neuronal activity in the dSTR. (*A*) Schematic illustration of in vivo real-time calcium activity recording. The right dSTR of mice was cotransduced by AAVs for a calcium sensor (hSyn:jRGECO1a) and hSyn:EYFP, hSyn:MscL-WT-EYFP, or hSyn:MscL-G22S-EYFP, at a 1:1 ratio. Four to five weeks later, anesthetized mice were stimulated with US, and neuronal calcium responses were recorded by an optical fiber implanted in the dSTR region. (*B*) Representative images of dSTR expressing hSyn:EYFP, hSyn:MscL-WT-EYFP or hSyn:MscL-G22S-EYFP, and hSyn:jRGECO1a. Caudoputamen (CP), cerebral cortex (CTX). Pink arrows indicate neurons coexpressing EYFP/MscL-WT/MscL-G22S and jRGECO1a. (*C*) An illustration of the ultrasound temporal profile used. The US parameters were: 0.5 MHz central frequency, 400 to 500 μs pulse width, 300 ms stimulation duration, 1 kHz PRF, 0.05 to 0.2 MPa pressure range. (*D*) Averaged jRGECO1a fluorescence traces in the dSTR of anesthetized EYFP, MscL-WT, and MscL-G22S mice prior to US stimulation (*Left*) and in response to one 0.05 MPa pressure ultrasound pulse (*Right*) (0.5 MHz center frequency, 500 μs pulse width, 300 ms stimulation duration, 1 kHz PRF, interval 3 s). Green rectangle shows the timing of ultrasound stimulation. (*E*) Average peak Ca^{2+} activity in EYFP, MscL-WT, and MscL-G22S mice in response to US pulses of varying intensities (0.05 to 0.2 MPa peak pressure, 500 μs pulse width, 0.5 MHz center frequency, 300 ms stimulation duration, 1 kHz PRF, interval 3 s). n = 8 mice, 14 trials in EYFP group, n = 4 mice, 8 trials in MscL-WT group, n = 5 mice, 6 trials in MscL-G22S group. **P* < 0.05, ***P* < 0.01, ****P* < 0.001, *****P* < 0.0001. Two-way ANOVA with Tukey' s multiple comparisons test. Data are shown as mean ± SEM. (*F*) Latency between US stimulation (0.05 to 0.2 MPa peak pressure) and detection of an above-threshold fluorescence change in MscL-G22S mice. n = 5. NS = not significant, one-way ANOVA with post-hoc Tukey test. Data are shown as mean ± SEM. (*G*) Representative images of dSTR following US stimulation (400 μs pulse width, 0.5 MHz center frequency, 300 ms stimulation duration, 1 kHz PRF, interval 10 s, 0.15 MPa). Images show DAPI + EYFP or MscL-G22S at low magnification (*Left*) and DAPI + c-Fos expression in the indicated areas at high magnification (*Right*). (*H*) Counts of nuclear c-Fos per slice imaged in the dSTR (*Left*) and the cortex above the targeted region (*Right*) of mice stimulated with ultrasound. n = 4 mice each group. Data are shown mean ± SEM of average c-Fos+ cells per stained slice. ****P* < 0.001, NS = not significant, one-way ANOVA with post-hoc Tukey test.

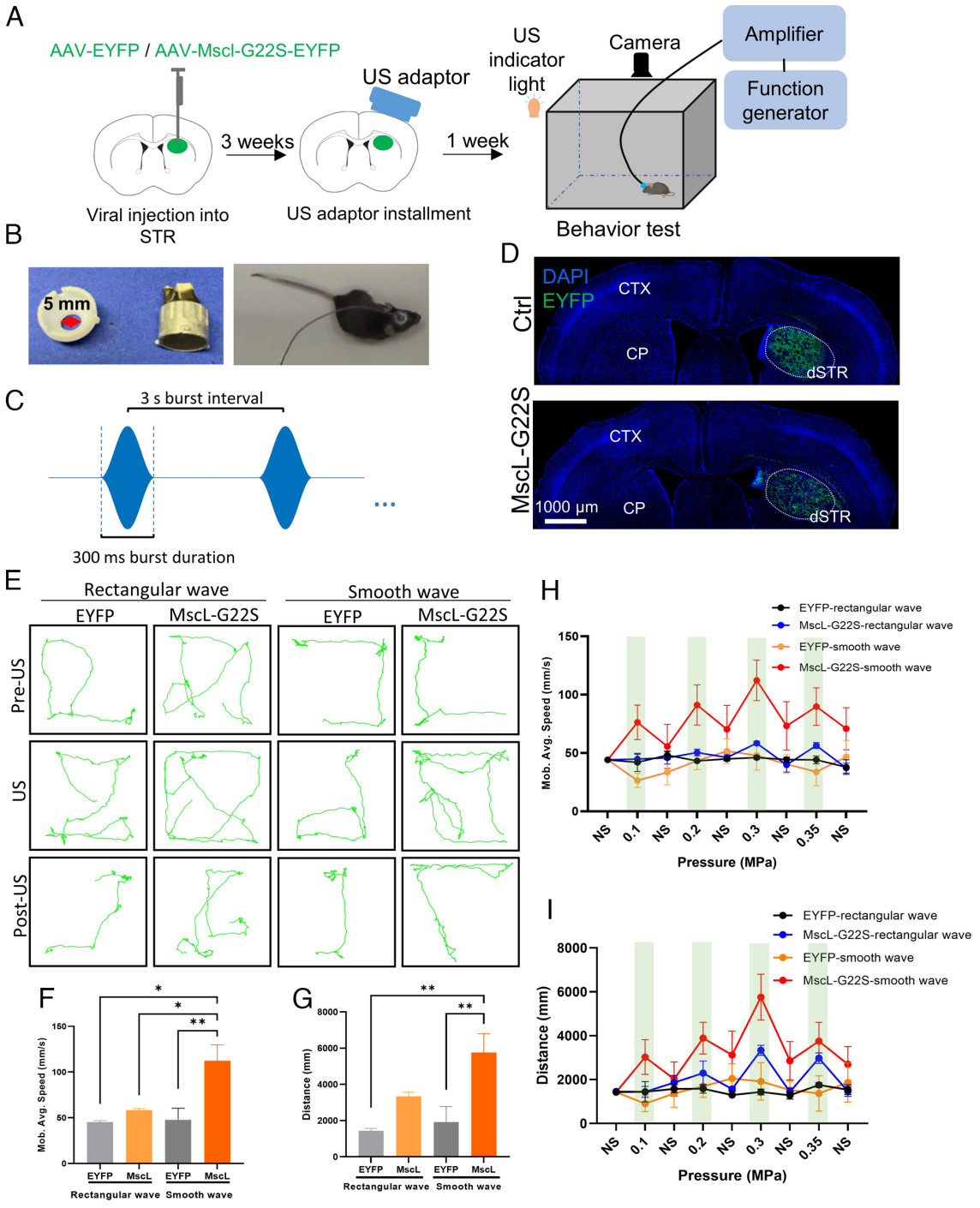

Fig. 2. Ultrasound stimulation evokes significantly greater locomotion in mice with MscL-expressing dSTR. (*A*) Schematic illustration of locomotion experiments. Briefly, mice were injected with hSyn:EYFP or hSyn:MscL-G22S in their right dSTR. Three weeks later, an ultrasound adaptor was installed. One week later, the mice were placed in an open-field box and their movements were recorded before, during, and after ultrasound stimulation. The behavior documented in the video was then analyzed and quantified. US parameters used were 1) rectangular waveform: 0.9 MHz central frequency, 400 μs pulse width, 300 ms duration, 1 kHz PRF, 0.1 to 0.35 MPa pressure ranges; 2) smooth waveform: 0.9 MHz central frequency, 300 ms duration, 0.1 to 0.35 MPa pressure ranges. (*B*) Images of the ultrasound adaptor and the wearable ultrasound transducer (*Left*). The diameter of the ultrasound adaptor was 5 mm. The wearable ultrasound transducer was mounted on the adaptor attached onto the mouse head (*Right*). (*C*) An illustration of the smooth-wave ultrasound profile used. US parameters were 0.9 MHz central frequency, 300 ms duration. (*D*) Representative images showing expression of DAPI + hSyn:EYFP (*Top*) or hSyn:MscL-EYFP (*Bottom*) in the dSTR. Caudoputamen (CP), cerebral cortex (CTX). (*E*) Representative trajectories recorded from mice stimulated in the dSTR pre-US, during US, and post-US with 0.3 MPa ultrasound application (each trace 1 min long). (*F*) Comparison of average speed of the EYFP and MscL mice during stimulation (0.3 MPa). For rectangular waveform: n = 5 mice in EYFP group, n = 6 mice in MscL-G22S group; for smooth waveform, n = 5 mice, 6 trials in EYFP group, n = 5 mice, 8 trials in MscL-G22S group. Data are shown as mean ± SEM; $^{*}P < 0.05$, $^{**}P < 0.01$. One-way ANOVA with Tukey's multiple comparisons test. (*G*) Summary of mobility average speed of EYFP and MscL mice with stimulation of different ultrasonic intensities from 0.1 to 0.35 MPa peak pressure. Green bars indicate the timing of ultrasonic stimuli. Data are shown as mean ± SEM; $^{**}P < 0.01$, One-way ANOVA with Tukey's multiple comparisons test. (*H*) Comparison of the horizontal distance covered by the same mice as in *E*. For rectangle waveform: n = 5 mice in EYFP group, n = 6 mice in MscL-G22S group; for smooth waveform, n = 5 mice, 6 trials in EYFP group, n = 5 mice, 8 trials in MscL-G22S group. Data are shown as mean ± SEM; Two-way ANOVA with Tukey's multiple comparisons test. (*I*) Summary of distance of EYFP- and MscL-expressing mice with stimulation of different ultrasonic pressures from 0.1 to 0.35 MPa peak pressure. Green bars indicate the timing of ultrasonic stimuli. Data are shown as mean ± SEM; Two-way ANOVA with Tukey's multiple comparisons test.

waveform of MscL-G22S mice showed more activities compared to rectangular waveform, supporting that the auditory confound could be minimized by smooth waveform to enhance the sonogenetic effect. Thus, MscL-sonogenetics in the dSTR could effectively induce significant motor responses of awake mice, consistent with previous optogenetic neuromodulation targeting the same region (14, 19).

Taken together, our findings suggest that MscL-sonogenetics can specifically stimulate neurons in the dSTR and induce the characteristic asymmetric locomotion behavior.

Efficient Dopamine Release and Appetitive Conditioning by MscL-Sonogenetic Modulation of VTA Reward Circuitry. We next tested the feasibility of using MscL-sonogenetics to control higher-level behavior by targeting more specific neurons. The VTA was chosen as it is a midbrain reward center where the dopaminergic (DA) circuit is well defined and involves in various reward-related behavior and diseases (20). In order to test whether MscL-sonogenetics could target specific circuits, DA VTA neurons were selectively made to express MscL-G22S. We used a dual-viral vector strategy: one vector delivered Cre recombinase under the modulation of a tyrosine hydroxylase promoter (TH promoter) (21, 22), and the other delivered a Cre-recombinase-dependent EYFP or MscL-G22S-EYFP fragment (Fig. 3*A*). Confocal imaging confirmed that TH^+ neurons overlapped with EYFP or MscL-G22S-EYFP in the VTA region (Fig. 3*B*), indicating successful expression of MscL-G22S in DA neurons.

We tested whether MscL-sonogenetics could specifically modulate appetitive conditioning using the real-time place preference assay. Habituated mice were placed in a rectangular open-field box with two distinct chambers, one paired with US stimulation, and the other paired without US stimulation (NUS), and the mice could move freely between chambers (Fig. 3*C*). The mice were wearing a transducer aimed at the VTA. US stimuli were triggered immediately when a mouse entered the US chamber and turned off immediately when the chamber was exited. Unexpectedly, we found that US stimulation induced aversive responses in EYFP mice starting at 0.07 MPa (*SI Appendix*, Fig. S4 *A* and *B*). In addition, increasing acoustic pressure to 0.16 MPa in EYFP mice induced further aversive behavior (*SI Appendix*, Fig. S4*B*). At the same time, MscL mice spent approximately equal time in both chambers for all pressures tested. Thus, we found that low US intensities affected appetitive condition in EYFP mice but not MscL-G22S mice, which might be due to nonspecific stimulation of the VTA or auditory confound.

Meanwhile, we conducted the real-time place preference test with smooth-waveform US. The smooth-waveform US was delivered to mice for the duration of their stay in the stimulation chamber. Upon making this change, we found no significant aversive effect in either group, while MscL mice spent an increased proportion of time in the stimulation-paired side with increasing US pressure 0.04 MPa to 0.12 MPa (Fig. 3 *D*–*F*). Thus, we found that sonogenetic stimulation of MscL-G22S-expressing mouse VTAs could specifically modulate appetitive conditioning.

Furthermore, we found that DA neuron–specific sonogenetic stimulation in the VTA could activate neuronal population in the NAc in acute ex vivo brain slices (*SI Appendix*, Fig. S5 *A* and *B*). NAc neurons displayed calcium fluorescence increases time-locked with the duration of when MscL-G22S-expressing VTA neurons were stimulated with US (*SI Appendix*, Fig. S5*C*), and responses from MscL-G22S neurons were significantly higher than those of EYFP neurons (*SI Appendix*, Fig. S5*D*). This suggests that expressing MscL-G22S in TH^+ VTA neurons enables sonogenetic stimulation of targeted cells by ultrasound. In summary, we found that US stimulation of mouse of MscL-G22S-expressing DA neurons in the VTA could modulate appetitive conditioning.

We also essayed to get direct confirmation of the VTA reward circuitry being activated through FP. Dopamine release following US stimulation was recorded in the NAc, downstream from the VTA in the mesolimbic pathway (23, 24). Neurons in the ipsilateral NAc were transduced with the fluorescent dopamine sensor hSyn:DA2m (25). An optical fiber was inserted into the NAc to monitor dopamine activity through the sensor's fluorescence change (Fig. 4*A*). We found robust DA2m expression in the NAc (*SI Appendix*, Fig. S6*A*) and MscL/EYFP signal in DA neurons of the VTA (*SI Appendix*, Fig. S6*B*). Upon stimulation of the VTA with pulse train of 0.3 MPa ultrasound, we found rapid synchronous increases in DA2m fluorescence in the NAc of the MscL mice but not EYFP mice (Fig. 4*B*). NUS and EYFP+US conditions at both tested US intensities showed very little fluorescence change, and the MscL + US conditions were larger in magnitude at both 0.1 MPa (peak $\Delta F/F_0$, EYFP = 0.18%, MscL = 0.42%) and 0.3 MPa (peak $\Delta F/F_0$, EYFP = 0.23%, MscL = 0.52%), although only the 0.3 MPa condition was statistically significant (Fig. 4*C*). DA signal responses to US stimuli were found to be repeatable and with a low latency of ~300 ms at both tested US intensities (Fig. 4 *D* and *E*). Taken together, our data suggest that MscL-sonogenetics could specifically induce DA secretion in neurons projecting to the NAc in vivo, eliciting place preference behavior.

In Vivo MscL-Sonogenetic Stimulation Alleviates Parkinsonian Symptoms in Freely Moving Mice. Given the ability of MscL-mediated ultrasound to activate the mesolimbic pathway, we wondered whether US stimulation could also have a beneficial effect on a neurological condition involving related pathways. We chose Parkinson's disease as our model and induced parkinsonian mice by unilateral injection of 6-OHDA (6-hydroxydopamine) into the brain. To specifically activate the neurons of subthalamus (STN), EYFP/MscL-G22S AAVs were injected into the STN region (*SI Appendix*, Fig. S7*A*). To test whether ultrasound stimulation could sensitize MscL-G22S-expressing STN neurons in PD mice, we performed EMG recording in the PD EYFP/MscL-G22S mice. We found that stimulation of MscL-expressing brains at low intensities could evoke hindlimb muscle contractions, with no or little response in the EYFP mice (*SI Appendix*, Fig. S7*B*). Both the magnitude of response (relative amplitude) and the rate of response were greater in MscL mice, and a general pattern of dose dependence was observed (*SI Appendix*, Fig. S7 *C* and *D*). At lower acoustic intensities, we observed no EMG response in the EYFP mice, with minor responses at higher acoustic pressures; however, MscL-G22S mice showed distinct responses at all tested intensities. In addition, we observed an increase in the nuclear c-Fos expression in the STN in MscL+PD mice (*SI Appendix*, Fig. S7 *E* and *F*). Thus, MscL-G22S expression could successfully sensitize STN neurons to ultrasound stimulation.

We then tested our sonogenetic protocol for alleviation of movement symptoms in parkinsonian mice. Rotating rod (rotarod) and open-field experiments were compared longitudinally in mice experiencing three conditions (baseline, before ultrasound stimulation, and after ultrasound stimulation, Fig. 5*A*). The mice were treated with US for 30 min/day for five consecutive days. As expected, unilateral 6-OHDA PD mice showed decrease in retention time in the rotarod test (baseline: EYFP mice = 78.29 ± 15.5 s, MscL mice = 90.2 ± 11.33 s, EYFP-PD mice = 16.7 ± 3.39 s, MscL-PD = 26.85 ± 5.46 s, Fig. 5*B*) and after the US stimulation regimen, a significant improvement was observed in the retention time of MscL+PD mice (US: EYFP-PD mice = 20.92 ± 4.60 s,

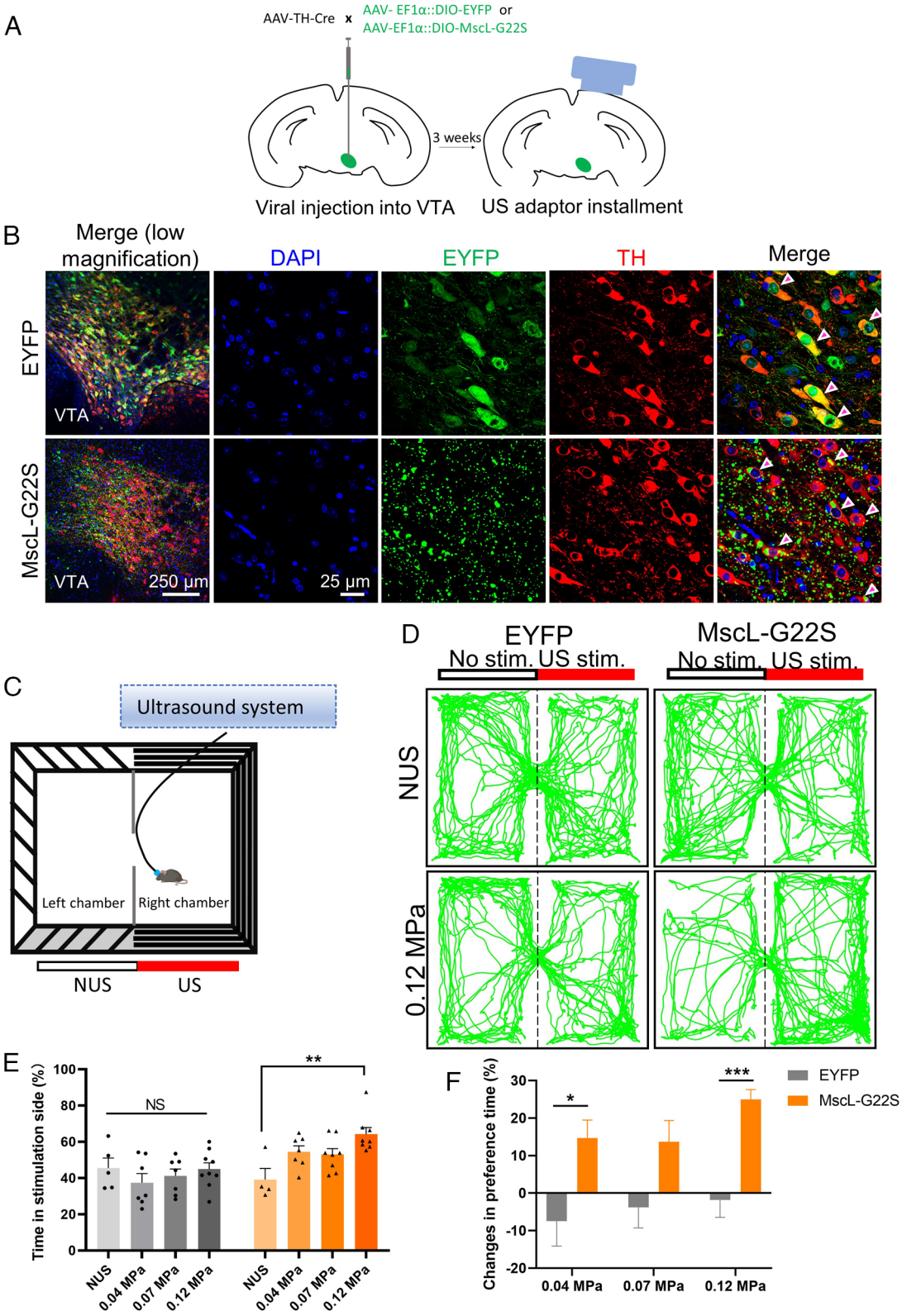

Fig. 3. Selective activation of mesolimbic pathway by MscL-sonogenetics enables appetitive conditioning. (*A*) Schematic illustration of the transduction protocol for DA neuron-specific transduction of MscL-G22S or EYFP. Briefly, mice were injected with a mix of AAV-TH-Cre and AAV-EF1α::DIO-EYFP or AAV-EF1α::DIO-MscL-G22S in the right VTA. Three weeks later, an ultrasound adaptor was installed followed by 1 wk for recovery, then the mice were stimulated with ultrasound. (*B*) Representative images depicting VTA regions expressing TH:EYFP (*Top*) or TH:MscL-G22S (*Bottom*). Arrows denote example EYFP+/TH+ neurons. (*C*) Schematic illustration of the real-time place preference assay. A two-chambered box was prepared, one chamber having horizontal stripes and the other with vertical stripes. The mice were habituated and tested according to the protocol illustrated. The movement of the mice between chambers was recorded by a digital camera (US = ultrasound, NUS = no ultrasound). (*D*) Representative path tracing of a mouse with TH-cre-EYFP (control) or TH-cre-MscL-EYFP expression during the real-time place preference test (0.12 MPa smooth wave). Red bar indicates stimulation side. (*E*) Calculated percentage of time spent by mice on the stimulation side with NUS, 0.04 MPa to 0.12 MPa US in control and MscL mice. n = 5 mice in control mice; n = 4 mice in MscL-expressing mice. Each mouse was subjected to 1 to 2 sonication trials. Each point indicates an independent trial. $^{**}P < 0.01$, two-way ANOVA with Sidak's multiple comparisons test. Data are shown as mean ± SEM. (*F*) Change in time spent by EYFP and MscL mice in the stimulation chamber upon US stimulation vs NUS condition. $^{*}P < 0.05$, $^{***}P < 0.001$, Two-way ANOVA with Sidak's multiple comparisons test. Data are shown as mean ± SEM.

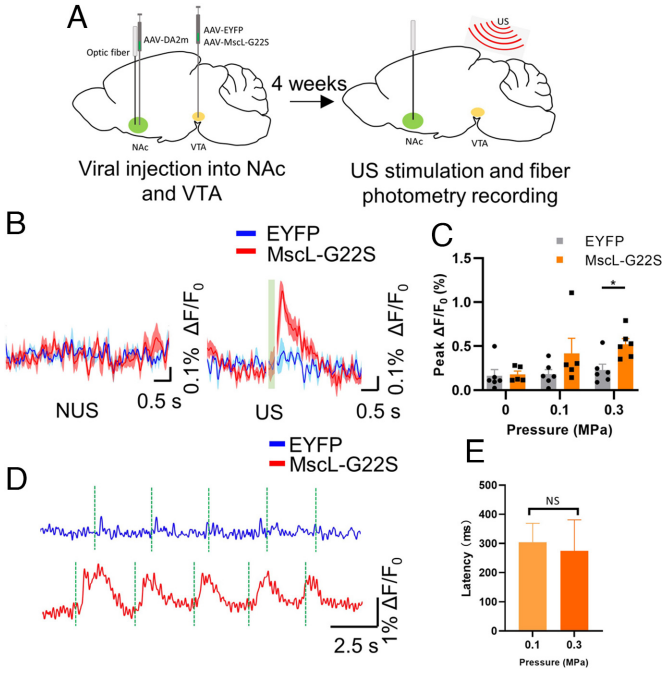

Fig. 4. Efficient sonogenetically enabled dopamine release in the NAc through modulation of the mesolimbic pathway. (*A*) Schematic illustration of dopamine FP experiments. Mice were injected with AAV-hSyn-DA2m in the right NAc and hSyn-EYFP or hSyn-MscL-EYFP in the ipsilateral VTA. After viral injection, an optical fiber was inserted into NAc. Four weeks later, the mice were treated with US and dopamine fluorescence signals were recorded. (*B*) Averaged DA2m fluorescence signal change ($\Delta F/F_0$) in the NAc of anesthetized EYFP- and MscL-expressing mice, with or without 0.3 MPa US stimulation. Blue traces show DA signals in the EYFP-expressing mice, while red traces show the DA signals in MscL-expressing mice. Green rectangle shows the timing of ultrasound stimulation. n = 4 mice, 6 trials/each in EYFP group. n = 5 mice, 6 trials/each in the MscL group. (C) Average peak DA2m activity ($\Delta F/F_0$) in response to 0, 0.1, 0.3 MPa ultrasound stimulation (0.5 MHz center frequency, 500 μs pulse width, 300 ms stimulation duration, 1 kHz PRF, interval 3s) in EYFP- and MscL-expressing mice. n = 6 trials from 4 mice in the EYFP group, n = 5 to 6 trials from 5 mice in the MscL-expressing group. *$P < 0.05$, multiple *t* test with Holm–Sidak correction. Data are shown as mean ± SEM. (*D*) Representative DA2m fluorescence traces in the NAc of anaesthetized EYFP- and MscL-expressing mice when stimulated by multiple pulse trains of 0.3 MPa US. (*E*) Latency between US stimulation and detection of an above-threshold fluorescence change in MscL mice. Data are shown as mean ± SEM. NS = not significant, unpaired two-tailed *t* test.

US: MscL-PD = 73.3 ± 9.33 s, Fig. 5*C*). In contrast, EYFP+PD mice did not show much change in performance after US stimulation (US: EYFP-PD mice = 60.16% ± 53.38%, US: MscL-PD = 258.1% ± 54.34%, Fig. 5*C*).

General motor functions were assessed in an open-field paradigm. Both groups of mice decreased their distance moved after the induction of PD, but following US stimulation, MscL mice covered significantly more distance than EYFP mice, indicating some rescue of motor function by sonogenetic stimulation in MscL+PS mice (US: EYFP-PD mice = −20.90% ± 4.76%, US: MscL-PD mice = 1.62% ± 5.67%, Fig. 5 *D*–*F*). A similar pattern was observed among these mice with regard to their mobile time. EYFP+PD mice exhibited a decline in mobile time between PD induction and completion of US treatment, but percentage mobile time of MscL+PD remained almost unchanged (US: EYFP-PD mice = −22.72% ± 3.67%, US: MscL-PD mice = −2.29% ± 4.55%, Fig. 5 *G* and *H*). The average speed of the mice was not significantly different between EYFP and MscL mice (*SI Appendix*, Fig. S8). Thus, we found that MscL-sonogenetics targeting the STN in PD mice could indeed rescue motor symptoms in parkinsonian mice.

Discussion

The present study demonstrates an MscL-G22S-mediated sonogenetic approach capable of stimulating specific neural circuits with high spatiotemporal precision, providing a noninvasive way to modulate higher behaviors in mouse models. Our setup proved capable of activating neurons and modifying characteristic motor behaviors and appetitive conditioning in conscious mice through the administration of low-intensity ultrasound. Real-time recording of neuronal responses to US pulse train in deep-brain regions of MscL-G22S mice through FP showed the rapid and reversible neuronal activation triggered by MscL-sonogenetics. Mutant MscL-G22S sensitizes neurons to ultrasound more effectively than wild-type MscL. The latency of fluorescence change was consistent between the genetically encoded calcium and dopamine sensors in the two regions, at ~300 ms. Although the temporal resolution of sonogenetics could not be determined by patch clamp, due to its incompatibility with ultrasonic vibrations, the quick responses measured by FP suggest a subsecond temporal precision. Moreover, MscL-sonogenetics could elicit well-defined behaviors through specific activation of established neural circuitry. Finally, the present study demonstrates the noninvasive sonogenetic modulation of the specific brain circuit in parkinsonian mice to alleviate the motor symptoms. Our stimulation scheme showed good spatiotemporal resolution when targeted to brain regions at different depths, without obvious nonspecific activation and responses closely synchronized with US stimuli.

Sonogenetics has the advantage of combining a modular element (the choice of mechanosensitive mediator) and a noninvasive stimulation modality (ultrasound). Some have raised concerns about the phenomenon of MscL channel clustering; however, it is reported that while MscL clustering could contribute to the nonuniform appearance of the GFP signal, this did not influence the cell viability and the ability of the channel to mediate mechanical stimuli (26). Here, we were able to further increase the specificity of the treatment by injecting virus in a specific brain region and using the Cre-Lox system to preferentially express MscL only in certain cell types. This combinatory approach offers multiple opportunities to tailor the treatment for the intended application and the prospect of continuous improvement. Choosing a different transducer or ultrasound parameters, different brain region, or a different cell type for targeting could allow the study of other aspects of brain function. The discovery and development of other mediating molecules, such as other mechanosensitive ion channels (6) or nonchannel transmembrane proteins (3), could provide ways to stimulate desired regions with ultrasound. It could also be possible to further reduce the invasiveness of the treatment by making use of genetic technologies. For instance, the AAV-PHP.eB virus has been shown to be capable of transducing cells in the brain through mere tail-vein administration (27, 28). Such a system could be used to preferentially transduce targeted cells in the brain while also possibly reducing the need to deliver the virus directly into the brain. Finally, we found MscL-sonogenetics to be compatible with FP and free-moving recording without significant interference and crosstalk. Thus, integration of these important techniques could help for comprehensive study of the brain and how it works. For instance, sonogenetics could further be used with fMRI, a well-established technique, and could thus enable screening and dissection of neural circuits in large animals, e.g., nonhuman primates. Thus, sonogenetics offers an adaptable, modular approach that is amenable to integration with other modalities, which could allow for wide-ranging study.

In addition to the modularity and noninvasiveness of the approach, another advantage of sonogenetics is that it can affect

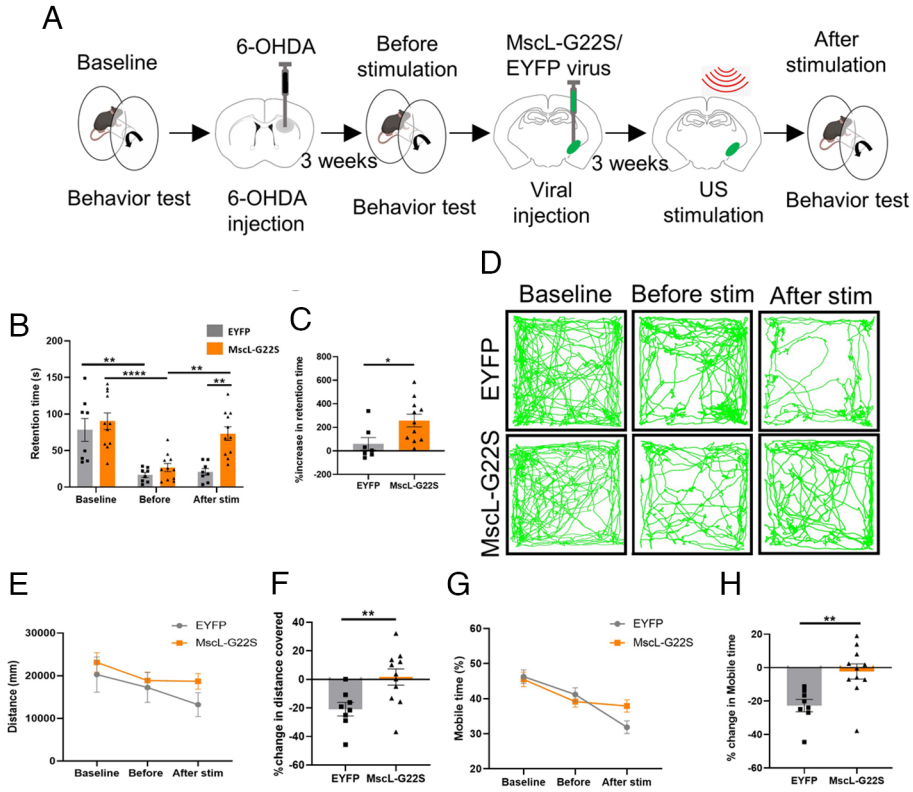

Fig. 5. Sonogenetic manipulation of STN improves motor coordination behavior in PD mice. (*A*) Schematic representation and timeline of 6-OHDA, virus injection, and behavioral experiments. US parameters were 500 kHz frequency, 400 μs pulse width, 300 ms duration, 1 ms pulse interval, 0.35 MPa. (*B*) Retention time(s) to fall from the rotarod apparatus in three conditions: baseline, after 6-OHDA infusion, and after sonogenetic treatment. n = 8 EYFP mice, n = 11 MscL mice, $^{**}P < 0.01$, $^{****}P < 0.0001$. Two-way ANOVA with post-hoc Tukey test. Data are shown as mean ± SEM. (*C*) Percentage increase in retention time following stimulation compared to prestimulus condition in EYFP mice and MscL mice. Data are shown as mean ± SEM. N = 8 EYFP mice, n = 11 MscL mice. $^{*}P < 0.05$, unpaired two-tailed *t* test with Welch's correction. (*D*) Representative 10 min movement traces in open-field arena observed in PD mice with MscL and EYFP expressed in the STN region. (*E*) Total distance traveled during 10 min in open field in the three conditions: baseline condition, after 6-OHDA infusion, and after sonogenetic activation. Data are shown as mean ± SEM. (*F*) Percentage increase in total distance traveled by PD mice, before vs after US stimulation. Data are shown as mean ± SEM. n = 8 EYFP mice, n = 11 MscL mice. $^{**}P < 0.01$, unpaired two-tailed *t* test with Welch's correction. (*G*) Percentage of time spent moving by mice when in the open-field apparatus. Movement at speeds of 20 mm/s and above during the observation period were recorded. Data are shown as mean ± SEM. (*H*) Percentage increase in the time spent mobile by PD mice, before vs after US stimulation. Data are shown as mean ± SEM. n = 8 EYFP mice, n = 11 MscL mice. $^{**}P < 0.01$, unpaired two-tailed *t* test with Welch's correction.

mesoscale circuits in the brain. Optogenetics has been used to dissect brain microcircuits affecting a specific brain function (29). However, understanding how these microcircuits interact and how higher-order functions are constituted would require modulation of mesoscale circuits. As shown here, with a flat single-element ultrasound transducer, MscL-sonogenetics can induce cell type–selective stimulation in the midbrain and deep brain dependent on the spatial profiles of MscL expression. Given the dynamic focusing capability of ultrasound transducers, sonogenetics could provide a way to stimulate mesoscale circuits noninvasively with defined spatiotemporal pattern to unlock complex signaling phenomena.

A potential concern about sonogenetics is the nonspecific activation of neurons, either through activating intrinsic mechanosensitive ion channels or stimulating peripheral auditory pathways causing background responses and compromising specificity and efficacy. Ultrasound has been shown to activate various endogenous mechanosensitive ion channels, including Piezo1 (30, 31), TRAAK (4), and TRPA1 (6). We tried to minimize nonspecific effects by using short US pulse train at the lowest effective acoustic pressure. Our application of sonogenetics in deeper brain regions, e.g., VTA and dSTR, did not show obvious off-target effects in the present study as measured by various assays, suggesting that MscL-sonogenetics is capable of stimulating specific neural circuits. However, the presence of endogenous mechanosensitive ion channels may narrow the window of usable pressures. Thus, it is necessary to improve the sensitivity of sonogenetic mediators and develop unique strategies for precise monitoring of acoustic pressure in situ. The place preference behavioral assay indicated that there was some auditory confound with rectangular waveforms. While the carrier frequency of the US pulse train we used was inaudible to mice, there could be audible wide-band noise at the on and off points of a rectangular waveform, which might induce auditory stimulation and the aversive behavior observed. Based on the Fourier transform theorem, the wide-band noise can be eliminated simply by smoothing the on- and off-set of a waveform (32). Our results support this concept as mice treated with smooth-wave US did not show significant aversive responses to US.

In addition, the underlying mechanisms of the ultrasonic effects on mechanosensitive ion channel are not fully understood. It has been shown that ultrasound can activate mechanically sensitive ion channels through deposition of acoustic radiation forces, thereby increasing membrane tension or deforming lipid bilayer geometry (33), and interaction with the cytoskeleton and components of the membrane bilayers (34), causing Ca^{2+} influx into the cells and affecting the neuronal activity (1, 35). More investigation needs to focus on the mechanisms of sonogenetics.

We envision that an approach like sonogenetics could be promising for the eventual development of neurological, neurodegenerative, or neuropsychiatric treatments. Unlike pharmacological

or lesion-based interventions, sonogenetics is noninvasive with cellular specificity and neural circuit accuracy. Regulating dopamine dynamics in the targeted region might help alleviate symptoms of such neurological diseases. In addition to dopamine, this approach may also regulate other neurotransmitters by manipulating specific neural circuits in appropriate brain regions, such as glutamatergic or GABAergic neurons. Thus, we believe that sonogenetic approach has the potential to become a unique alternative approach for treating neurological and psychiatric diseases.

Materials and Methods

Animal Subjects. Male, 6 to 8-wk-old, C57BL/6J mice, were used for this study. The mice were housed under standard conditions with food and water available ad libitum. The mice were habituated to the procedure room for at least 30 min prior to behavioral testing experiments. All animal experiments were approved by the Animal Subjects Ethics Sub-Committee (ASESC) of the Hong Kong Polytechnic University. Animal use and care were performed following the guidelines of the Department of Health – Animals (Control of Experiments) of the Hong Kong S.A.R. government.

Stereotaxic Injection of AAVs. Mice were anesthetized with ketamine and xylazine (100 mg/kg and 10 mg/kg respectively) and placed in a stereotaxic instrument (RWD, Shenzhen, China). A small craniotomy hole was made over the targeted area. Viral vectors were microinjected into the right side of the mouse brain by standard stereotaxic procedures (36). AAVs were injected at the rate of 0.05 to 0.1 μL per minute. The microsyringe was left in place for an extra 10 min before withdrawal.

For locomotion experiments, 500 nL AAV-hSyn-EYFP or AAV-hSyn-MscL-G22S-EYFP (BrainVTA (Wuhan) Co. Ltd) was unilaterally injected into the dSTR at AP +0.50 mm, ML −1.8 mm, from Bregma and DV −2.75 mm from the brain surface. Three weeks posttransduction, a portion of the scalp was excised at the above coordinates, and an ultrasound adaptor was fixed to the skull using dental cement.

For calcium FP in the dSTR, mice were injected with virus vectors in the right side of the dSTR (DV: −2.75 mm) as mentioned above. The volume ratio of the viral vector mixture was 1:1 for AAV-hSyn-jRGECO1a (OBiO Technology, Shanghai), AAV-hSyn-EYFP, AAV-hSyn-MscI G22S-EYFP, or hSyn-MscL-WT-EYFP (Brain Case, Shenzhen) in the dSTR. After microsyringe withdrawal, an optic fiber was inserted into the location of the syringe.

For dopamine FP in the VTA, 300 nl AAV-hSyn-EYFP or AAV-hSyn-MscI-G22S-EYFP was microinjected into the right side of the VTA (AP: −2.9 mm, ML: −0.5 mm, DV: −4.5 mm), and 1 μL hSyn-DA2m (Vigene Bioscience Co., Ltd) was injected into the ipsilateral side of nucleus accumbens (NAc, coordination: AP: 1 mm, ML: −1.1 mm, DV: −4.1 mm). An optical fiber was implanted in the NAc region after AAV injection.

For reward-related experiments (real-time place preference), 300 nL AAV-EF1a::DIO-EYFP or AAV-EF1a::DIO-MscL-G22s-EYFP [BrainVTA (Wuhan) Co. Ltd] mixed with pAAV-TH-Cre-WPRE-hGHpA (OBiO Technology, Shanghai) (1:1) was microinjected into the right side of the VTA (AP: −2.9 mm, ML: −0.5 mm, DV: −4.5 mm). An ultrasound adaptor was installed above the targeted region after 3 wk of viral transduction.

For the VTA and NAc acute brain slice calcium imaging experiment, 300 nL AAV-EF1a::DIO-EYFP or AAV-EF1a::DIO-MscL-G22s-EYFP mixed with pAAV-TH-Cre-WPRE-hGHpA (1:1) was microinjected into the right side of the VTA (AP: −2.9 mm, ML: −0.5 mm, DV: −4.5 mm), and 0.5 μL hSyn-jRGECO1a was injected into the ipsilateral side of NAc (AP: 1 mm, ML: −1.1 mm, DV: −4.1 mm).

For PD experiment, 1 μL 6-OHDA was unilaterally injected into the right dorsomedial striatum (DMS, AP: +0.5 mm, ML: −1.5 mm, DV: −2.0 mm). Three weeks later, 500 nL AAV-hSyn-EYFP or AAV-hSyn-MscL-G22S-EYFP was unilaterally injected into SNT (AP: −1.95 mm; ML: −1.65 mm; DV: −4.3 mm).

Ultrasound Instrument and Transducer Installation. Ultrasound transducer (I7-0012-P-SU, Olympus or wearable transducer) was driven by a set of function generators (DG4102, Rigol; Tektronix AFG3251, Agilent Technologies) and power amplifier (A075, Electronics & Innovation Ltd), generating pulsed ultrasound with 0.5 MHz or 0.9 MHz central frequency, 1 kHz PRF, 40% or 50% duty cycle, under burst mode at 300 ms duration. Alternatively, a smoothed waveform was generated at 3 s interval using the same setup, where 300 ms of continuous ultrasound with 0.9 MHz central frequency was smoothed by a Hann window of the same length. The skull above the targeted region was cleaned with saline. A wearable ultrasound transducer was mounted upon the adaptor attached to the skull, coupled with ultrasound gel.

Thermal Simulation. A commercial finite-element analysis software (COMSOL Multiphysics 6.0) was used to simulate the thermal response of biological tissue in acoustic field. The geometry was axisymmetrically modeled with the aperture of 50 mm. Physical field for water was selected as *pressure acoustics–frequency domain* to accurately simulate the propagation of acoustic waves. To simulate the infinite water domain and avoid the influence of nonexperimental factors, a perfect matching layer was selected on the outermost side of the model. After that, a sufficiently small mesh (less than λ/5, λ wavelength at center frequency) was divided, and the frequency of 0.5 MHz was applied to simulate the acoustic field. At last, based on the calculated acoustic intensity distribution, physical field for tissue [density: 1,044 kg/m^3; sound speed: 1,568 m/s; thermal conductivity: 0.59 W/(m·K); heat capacity: 3,710 J/(kg·K)] was selected as *biological heat transfer* to simulate thermal response caused by ultrasound.

FP Recording. FP recordings were performed at least 4 wk after viral injection. Mice (jRGECO1a- or DA2m-expressing mice) were anesthetized with 1 to 2% isoflurane and the hair was removed with scissors. Eye ointment was applied to prevent corneal drying. The implanted fiber was connected to a fiber-optic meter (Thinker Tech Nanjing BioScience Inc.) through an optical fiber patch cord for guiding the light. FP recoding was performed using a 570-nm laser at around 50 μW for jRGECO1a and a 480-nm laser at around 50 μW for DA2m. Data were collected at 100 Hz and analyzed using a customized MATLAB script. The fluorescence change ($\Delta F/F_0$) was calculated as $(F-F_0)/F_0$, where F_0 is the baseline fluorescence signal. The 0.2% increase in the magnitude was set as onset time (35).

Open-Field Recording of Locomotion. In mice with transduced dSTR regions, 1 wk after adaptor installation, a 0.9-MHz wearable ultrasound transducer was plugged into it. The mice were placed into the center of an open-field chamber (40 cm length × 40 cm width × 30 cm height). The mice were habituated in the chamber for 15 to 20 min prior to ultrasound stimulation. Mouse movements were then captured by a digital camera (Canon, LEGRIA, HF, M506) placed at ~45 cm above the open-field chamber. The mice were allowed to rest 1 to 3 min between each trial. The total travel distance and the mobility speed of mice were calculated from the recorded video clips using ToxTrac software (37, 38) and normalized to that of the same distance/mobility speed on the first average measurement. A mouse was considered to be moving at a minimum speed of 20 mm/s.

For the PD experiment, the locomotor behaviors of mice were monitored in the open-field box before 6-OHDA injection (referred to as the "baseline"). Three weeks postinjection with 6-OHDA, the movements of mice were recorded in the same box (referred to as "before ultrasound stimulation"). Three weeks posttransduction with EYFP/MscL viruses, the mice were treated with ultrasound for 30 min/d for five consecutive days (referred to as "after ultrasound stimulation") and then subjected to open-field behavioral observation. The total travel distance and the mobility speed of mice in the above three conditions were compared as an assessment of the therapeutic effect of MscL-sonogenetics on PD mice. The total travel distance and average mobility speed of mice were calculated using the method mentioned in the previous paragraph. The performance of individual PD mice was tracked and compared over the course of the experiment to obtain an accurate idea of the degree of improvement.

Real-Time Place Preference Assay. A 50 × 60-cm arena was divided into left and right chambers of equal size (50 cm length × 30 cm width × 30 cm height). The walls on each side were marked with horizontal stripes or vertical stripes. Mice were allowed to habituate in the arena on day 0. The mice were then stimulated with the ultrasound apparatus at 0, 0.1, or 0.3 MPa per daily session until completion of the experiment. The mice were allowed to freely explore the two chamber arenas for 20 min. One chamber was randomly assigned as being the stimulation chamber. When a mouse entered the stimulation chamber, ultrasound delivery was immediately begun, until it crossed over to the nonstimulation chamber, at which point the US was immediately stopped. The movement of the mice was recorded via a digital camera (Logitech 720p), and the time of the mice spent in each chamber (stimulated and nonstimulated) was calculated using the ToxTrac program.

Rotarod Test. Mice were habituated to the rotarod rotating bars (LE8505) and were pretrained for three trials at 5 rpm, 10 rpm, and 15 rpm. During testing, three trials were performed at 15 rpm and the average retention time was recorded. Untreated mice having at least 30 s retention time were chosen for 6-OHDA injection and further studies. Rotarod behavior tests in each mouse were performed in three cases (baseline, before ultrasound stimulation, and after ultrasound stimulation). Motor performance was also assessed using an accelerated rotarod protocol, going from 4 to 40 rpm in 40 s. Trials were begun by placing a mouse on the rod and beginning rotation. Each testing session comprised three trials and each trial ended when the mouse fell off the rod, and the rpm at which the mouse fell was recorded.

EMG Recording in Anesthetized Mice and Data Processing. Four to five weeks postinjection, mice with EYFP/MscL-G22S viruses in their right STN regions each were anesthetized with 2% isoflurane and eye ointment was applied to both eyes. Two EMG electrodes were inserted approximately 3 to 5 mm apart into the gastrocnemius muscle of the left hindlimb to record bioelectric potential difference across the muscle tissue. An EMG ground wire was attached to the ear of the animal. Isoflurane level was reduced to 0.5% 5 min before starting EMG recording. Ultrasound stimulation (500 kHz frequency, 400 μs pulse width, 300 ms stimulation duration, 1 ms pulse interval) with pressures 0.05 to 0.70 MPa was performed on each mouse. Each round consisted of 7 to 10 ultrasound stimuli delivered at an interval of 5 s. Each mouse was allowed 1 min rest between multiple rounds of stimulation. EMG signals were collected with a multichannel signal acquisition system (Medus, Bio-Signal Technologies). EMG data were analyzed using MATLAB (The MathWorks, Inc.). Raw EMG data were first filtered using a 50-Hz notch filter. Then, the signals were filtered with 10 Hz, 4th-order high-pass Butterworth filter, followed by 200 Hz, 4th-order Butterworth low-pass filter. The 3.5 s rectified filtered signal during each US pulse train delivery (from 0.5 s to 2 s after stimulation) was assessed for peak amplitude. US stimulation is considered as success if the US pulse train increases the amplitude by at least three times the prestimulation baseline condition.

Immunohistochemical Fluorescent Staining of c-Fos. Ninety minutes after ultrasound treatment, mice were perfused with 0.9% saline, followed by 4% paraformaldehyde (PFA) (cat. no. P1110, Solarbio). After dissection, the brains were postfixed overnight in 4% PFA. Coronal sections were prepared from the brain at a thickness of 40 μm by a vibratome. Slices were blocked using blocking buffer (10% normal goat serum + 1% BSA + 0.3% Triton in 1× PBS) and incubated overnight in primary antibody solution diluted in the blocking buffer. The slices were then washed with PBS three times and incubated with secondary antibodies diluted in blocking buffer for two hours at room temperature. The slices were then washed three times and coverslips were dried and mounted on glass slides using small drops of Prolong Diamond Antifade Mountant with DAPI. Primary antibodies used were c-Fos (2250, Cell Signaling Technology, dilution 1:500) and tyrosine hydroxylase (MAB318, Millipore, dilution 1:500). Secondary antibodies used were goat anti-rabbit IgG (H+L), Alexa Fluor 555 (A-21428, Invitrogen, dilution1:1,000) or goat anti-mouse IgG (H+L), and Alexa Fluor 555 (A-32727, Invitrogen, dilution 1:1,000). Each sample was divided into three sets and one set was used to stain for c-Fos expression. Each set contained 5 to 8 brain slices. The number of cells showing c-Fos was counted using ImageJ, and the number of c-Fos$^+$ cells per 733 × 733 μm slice was calculated. All brain slices were imaged using the confocal microscope (TCS SP8, Leica) in the University Research Facility in Life Sciences facilities in The Hong Kong Polytechnic University. Also, Nikon eclipse Ti2-E Live-cell fluorescence imaging system was used to get the whole-brain pictures.

Preparation and Fluorescence Imaging of Acute Brain Slices. Four weeks after virus injection, mice were anesthetized with an intraperitoneal injection of ketamine and xylazine (100 mg/kg and 10 mg/kg, respectively) and perfused with ice-cold oxygenated NMDG ACSF buffer containing (in mM): 92 N-methyl-D-glucamine (NMDG), 2.5 KCl, 1.25 NaH2PO4, 20 NaHCO3, 10 HEPES, 25 glucose, 2 thiourea, 5 Na-ascorbate, 3 Na-pyruvate, 0.5 CaCl2, 10 MgSO2, and 12 NAc. The pH of the ASCF was 7.3 to 7.4. The brains were immediately removed and placed in ice-cold oxygenated slicing buffer. The brains were sectioned into 300 um thick slices using vibratome (Leica VT1200), and the slices were incubated at 34 °C in NMDG ACSF for 10 to 12 min, followed by N-2-hydroxyethylpiperazine-N-2-ethanesulfonic acid (HEPES) ACSF that contained (in mM): 92 NaCl, 2.5 KCl, 1.25 NaH2PO4, 30 NaHCO3, 20 HEPES, 25 glucose, 2 thiourea, 5 Na-ascorbate, 3 Na-pyruvate, 2 CaCl2, and 2 MgSO2 for at least 1 h at 25 °C. The brain slices were transferred to a slice chamber for calcium fluorescence imaging and were continuously perfused with standard ACSF that contained (in mM): 119 NaCl, 2.5 KCl, 1.25 NaH2PO4, 24 NaHCO13, 1.25 glucose, 2 CaCl2, and 2 MgSO2 at 2 to 3 mL/min. An ultrasound transducer with a plastic tube was placed above the VTA region, and the neural activity of NAc neurons was recorded by a modified inverted epifluorescence microscope. The fluorescence was recorded using a 575 to 645-nm filter.

Data Processing. The counting of c-Fos$^+$ cells per slice was single blinded, performed by an experimenter who did not know the groups beforehand.

Behavioral tests' data analysis was done by experimenters blinded to experimental conditions using the ToxTrac program.

Statistical Analysis. All statistical analyses were performed using the GraphPad Prism software. Two-tailed unpaired *t* tests and one- or two-way ANOVA, with post-hoc Tukey or Holm–Sidak test as appropriate, were performed to determine statistical significance. The individual test performed for any graph is specified in the corresponding figure legend. Summary results were presented as mean ± SEM. *P* values below 0.05 were considered statistically significant.

Data, Materials, and Software Availability. All study data are included in the article and/or *SI Appendix*. The data have been deposited in the figshare repository and can be downloaded from the following URL: https://figshare.com/articles/dataset/Xian_Data_for_Modulation_of_deep_neural_circuits_with_sonogenetics_/22776362 (39).

ACKNOWLEDGMENTS. This work was supported by Guangdong High-Level Innovation Research Institute (2021B0909050004), Hong Kong Research Grants Council General Research Fund (15104520, 15102417, and 15326416), Hong Kong Innovation Technology Fund (MRP/018/18X and MHP/014/19), Shenzhen-Hong Kong-Macau Science and Technology Program (SGDX20201103095400001), Key-Area Research and Development Program of Guangdong Province (2018B030331001), and internal funding from the Hong Kong Polytechnic University (1-ZVW8 and 1-CD76). We would like to thank the facilities and technical support from University Research Facility in Life Sciences and University Research Facility in Behavioral and Systems Neuroscience of The Hong Kong Polytechnic University.

Author affiliations: [a]Department of Biomedical Engineering, The Hong Kong Polytechnic University, Hung Hom, Hong Kong SAR 999077, P.R. China; [b]Guangdong Institute of Intelligence Science and Technology, Hengqin, Zhuhai, Guangdong 519031, P.R. China; and [c]Paul C. Lauterbur Research Center for Biomedical Imaging, Institute of Biomedical and Health Engineering, Shenzhen Institutes of Advanced Technology, Chinese Academy of Sciences, Shenzhen 518055, P.R. China

1. Z. Qiu *et al.*, Targeted neurostimulation in mouse brains with non-invasive ultrasound. *Cell Rep.* **32**, 108033 (2020).
2. S. Ibsen *et al.*, Sonogenetics is a non-invasive approach to activating neurons in Caenorhabditis elegans. *Nat. Commun.* **6**, 1–12 (2015).
3. Y.-S. Huang *et al.*, Sonogenetic modulation of cellular activities using an engineered auditory-sensing protein. *Nano Lett.* **20**, 1089–1100 (2019).
4. B. Sorum *et al.*, Ultrasound activates mechanosensitive TRAAK K+ channels through the lipid membrane. *Proc. Natl. Acad. Sci. U.S.A.* **118**, e2006980118 (2021).
5. Y. Yang *et al.*, Sonothermogenetics for noninvasive and cell-type specific deep brain neuromodulation. *Brain Stimul.* **14**, 790–800 (2021).
6. M. Duque *et al.*, Sonogenetic control of mammalian cells using exogenous Transient Receptor Potential A1 channels. *Nature communications* **13**, 600 (2022).
7. T. Liu *et al.*, Sonogenetics: Recent advances and future directions. *Brain Stimul.* **15**, 1308–1317 (2022).
8. J. Ye *et al.*, Ultrasonic control of neural activity through activation of the mechanosensitive channel MscL. *Nano Lett.* **18**, 4148–4155 (2018).
9. B. Martinac, Mechanosensitive ion channels: Molecules of mechanotransduction. *J. Cell Sci.* **117**, 2449–2460 (2004).
10. S. Sukharev *et al.*, The gating mechanism of the large mechanosensitive channel MscL. *Nature* **409**, 720–724 (2001).
11. E. D'Angelo, S. Casali, Seeking a unified framework for cerebellar function and dysfunction: From circuit operations to cognition. *Front. Neural. Circuits.* **6**, 116 (2013).
12. G. Cui *et al.*, Concurrent activation of striatal direct and indirect pathways during action initiation. *Nature* **494**, 238–242 (2013).

13. G. Barbera *et al.*, Spatially compact neural clusters in the dorsal striatum encode locomotion relevant information. *Neuron* **92**, 202–213 (2016).
14. L. A. V. Magno *et al.*, Optogenetic stimulation of the M2 cortex reverts motor dysfunction in a mouse model of Parkinson's Disease. *J. Neurosci.* **39**, 3234–3248 (2019).
15. T. Miyazaki, Large timescale interrogation of neuronal function by fiberless optogenetics using lanthanide micro-particles. *Cell Rep.* **26**, 1033–1043.e5 (2019).
16. M. W. Howe, D. A. Dombeck, Rapid signalling in distinct dopaminergic axons during locomotion and reward. *Nature* **535**, 505–510 (2016).
17. H. Dana *et al.*, Sensitive red protein calcium indicators for imaging neural activity. *Elife* **5**, e12727 (2016).
18. M. Mohammadjavadi *et al.*, Elimination of peripheral auditory pathway activation does not affect motor responses from ultrasound neuromodulation. *Brain Stimul.* **12**, 901–910 (2019).
19. A. V. Kravitz *et al.*, Regulation of parkinsonian motor behaviours by optogenetic control of basal ganglia circuitry. *Nature* **466**, 622–626 (2010).
20. S. Lammel *et al.*, Input-specific control of reward and aversion in the ventral tegmental area. *Nature* **491**, 212–217 (2012).
21. W. R. Stauffer, Dopamine neuron-specific optogenetic stimulation in rhesus macaques. *Cell* **166**, 1564–1571.e6 (2016).
22. H. S. Gompf *et al.*, Targeted genetic manipulations of neuronal subtypes using promoter-specific combinatorial AAVs in wild-type animals. *Front. Behav. Neurosci.* **9**, 152 (2015).
23. T. M. Tzschentke, W. J. Schmidt, Functional relationship among medial prefrontal cortex, nucleus accumbens, and ventral tegmental area in locomotion and reward. *Crit. Rev. Neurobiol.* **14**, 131–142 (2000).
24. M. J. Wanat *et al.*, Phasic dopamine release in appetitive behaviors and drug addiction. *Curr. Drug Abuse Rev.* **2**, 195–213 (2009).
25. F. Sun *et al.*, A genetically encoded fluorescent sensor enables rapid and specific detection of dopamine in flies, fish, and mice. *Cell* **174**, 481–496.e19 (2018).
26. S. L. Grage *et al.*, Bilayer-mediated clustering and functional interaction of MscL channels. *Biophys. J.* **100**, 1252–1260 (2011).
27. K. Y. Chan *et al.*, Engineered AAVs for efficient noninvasive gene delivery to the central and peripheral nervous systems. *Nat. Neurosci.* **20**, 1172–1179 (2017).
28. R. D. Dayton *et al.*, More expansive gene transfer to the rat CNS: AAV PHP. EB vector dose–response and comparison to AAV PHP. B. *Gene Therapy* **25**, 392–400 (2018).
29. J. Apergis-Schoute *et al.*, Optogenetic evidence for inhibitory signaling from orexin to MCH neurons via local microcircuits. *J. Neurosci.* **35**, 5435–5441 (2015).
30. M. L. Prieto *et al.*, Activation of Piezo1 but not NaV1. 2 channels by ultrasound at 43 MHz. *Ultrasound Med. Biol.* **44**, 1217–1232 (2018).
31. Z. Qiu *et al.*, The mechanosensitive ion channel Piezo1 significantly mediates in vitro ultrasonic stimulation of neurons. *iScience* **21**, 448–457 (2019).
32. T. Sato *et al.*, Ultrasonic neuromodulation causes widespread cortical activation via an indirect auditory mechanism. *Neuron* **98**, 1031–1041.e5 (2018).
33. J. Blackmore *et al.*, Ultrasound neuromodulation: A review of results, mechanisms and safety. *Ultrasound Med. Biol.* **45**, 1509–1536 (2019).
34. M. Duque *et al.*, Sonogenetic control of mammalian cells using exogenous Transient Receptor Potential A1 channels. *Nat. Commun.* **13**, 600 (2022).
35. S. Yoo *et al.*, Focused ultrasound excites cortical neurons via mechanosensitive calcium accumulation and ion channel amplification. *Nat. Commun.* **13**, 493 (2022).
36. A. Cetin *et al.*, Stereotaxic gene delivery in the rodent brain. *Nat. Protoc.* **1**, 3166–3173 (2006).
37. A. Rodriguez *et al.*, ToxTrac: A fast and robust software for tracking organisms. *Methods Ecol. Evol.* **9**, 460–464 (2018).
38. A. Rodriguez *et al.*, ToxId: An efficient algorithm to solve occlusions when tracking multiple animals. *Sci. Rep.* **7**, 1–8 (2017).
39. Q. Xian *et al.*, Data files from "Modulation of deep neural circuits with sonogenetics". FigShare. https://figshare.com/articles/dataset/Xian_Data_for_Modulation_of_deep_neural_circuits_with_sonogenetics_/22776362. Deposited 11 May 2023.